Catalysis Letters (2018) 148:3062–3071
https://doi.org/10.1007/s10562-018-2491-4

Impregnated and Co-precipitated Pd–Ga_2O_3, Pd–In_2O_3 and Pd–Ga_2O_3–In_2O_3 Catalysts: Influence of the Microstructure on the CO_2 Selectivity in Methanol Steam Reforming

Christoph Rameshan[1,3,5] · Harald Lorenz[1] · Marc Armbrüster[2] · Igor Kasatkin[3,4] · Bernhard Klötzer[1] · Thomas Götsch[1] · Kevin Ploner[1] · Simon Penner[1]

Received: 14 February 2018 / Accepted: 15 July 2018 / Published online: 3 August 2018

Abstract

To focus on the influence of the intermetallic compound—oxide interface of Pd-based intermetallic phases in methanol steam reforming (MSR), a co-precipitation pathway has been followed to prepare and subsequently structurally and catalytically characterize a set of nanoparticulate Ga_2O_3- and In_2O_3-supported $GaPd_2$ and InPd catalysts, respectively. To study the possible promoting effect of In_2O_3, an In_2O_3-doped Ga_2O_3-supported $GaPd_2$ catalyst has also been examined. While, upon reduction, the same intermetallic compounds are formed, the structure of especially the Ga_2O_3 support is strikingly different: rhombohedral and spinel-like Ga_2O_3 phases, as well as hexagonal $GaInO_3$ and rhombohedral In_2O_3 phases are observed locally on the materials prior to methanol steam reforming by high-resolution transmission electron microscopy. Overall, the structure, phase composition and morphology of the co-precipitated catalysts are much more complex as compared to the respective impregnated counterparts. However, this induces a beneficial effect in activity and CO_2 selectivity in MSR. Both Ga_2O_3 and In_2O_3 catalysts show a much higher activity, and in the case of $GaPd_2$–Ga_2O_3, a much higher CO_2 selectivity. The promoting effect of In_2O_3 is also directly detectable, as the CO_2 selectivity of the co-precipitated supported Ga_2O_3–In_2O_3 catalyst is much higher and comparable to the purely In_2O_3-supported material, despite the more complex structure and morphology. In all studied cases, no deactivation effects have been observed even after prolonged time-on-stream for 12 h, confirming the stability of the systems.

Graphical Abstract

The presence of a variety of distinct supported intermetallic InPd and $GaPd_2$ particle phases is not detrimental to activity/selectivity in methanol steam reforming as long as the appropriate intermetallic phases are present and they exhibit optimized intermetallic-support phase boundary dimensions.

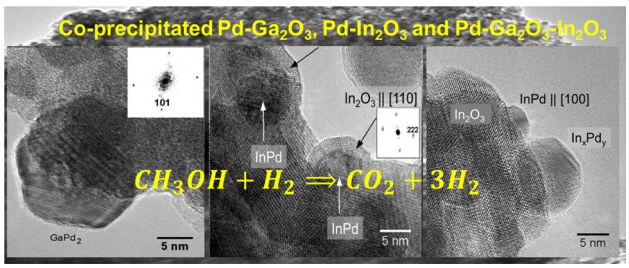

Keywords X-ray diffraction · High-resolution electron microscopy · Catalysis · Intermetallic compound · Hydrogen reduction · Catalyst activation

✉ Simon Penner
simon.penner@uibk.ac.at

Extended author information available on the last page of the article

1 Introduction

Pd-based intermetallic compounds have long been in the focus of research due to their outstanding catalytic properties in methanol steam reforming [1–5]. The associated high CO_2-selectivity has tentatively been ascribed to the general presence of the intermetallic compound after reduction in hydrogen, whose electronic structure mimics that of the technologically used Cu/ZnO catalysts [6]. It is now widely accepted that the mere presence of the intermetallic compound alone is not sufficient to explain the high CO_2 selectivity, but rather, the close contact to the oxide phase is a prerequisite for efficient water activation, the crucial step in obtaining high CO_2 selectivities [7–9]. Among the studied systems, $GaPd_2$/Ga_2O_3 [10–16], ZnPd/ZnO [5, 17–21] and InPd/In_2O_3 [22–24] have been scrutinized most and many of their structural, physico-chemical and catalytic properties have been already determined satisfactorily. As the simultaneous presence of both intermetallic compound and (partially reduced) oxide supports (monoclinic Ga_2O_3, hexagonal ZnO and cubic In_2O_3, respectively) is of utmost importance to induce a bifunctional synergism and, thus, to obtain high CO_2 selectivities, to search for synthesis methods in order to obtain a potentially larger intermetallic-oxide interface concentration is imperative. So far, apart from thin film or other model catalyst approaches [4, 7, 8, 14, 19–22], preparation of those catalysts is basically performed using standard incipient wetness impregnation pathways.

In this work, to increase the supposedly catalytically active interface, we follow a Pd and Ga_2O_3 and In_2O_3 co-precipitation approach using nitrate precursor solutions, respectively. In due course, the structure and catalytic properties are directly compared to their impregnated counterparts. The present work also focuses on the possible difference between using either Ga_2O_3 or In_2O_3 as active catalyst support, because Ga_2O_3-containing catalysts are known to exhibit a significantly lower CO_2 selectivity as compared to their In_2O_3-containing counterparts. This task is tackled by deliberately promoting a Pd–Ga_2O_3 catalyst with In_2O_3 in the co-precipitation process. Additionally, we present long-term activity measurements for the entire set of catalysts to elucidate deactivation, an undesired catalytic property that has not been addressed in detail for this class of materials so far. Special attention will be given to a detailed comparison of the structure and morphology of both (inter) metallic and oxide particles before and after the methanol steam reforming treatment, thus extensive high-resolution electron microscopy experiments are an integral part of the work.

2 Experimental

2.1 Catalyst Preparation

In order to suppress a potential influence of the preparation routine on the catalytic properties, the synthesis protocols were kept as similar as possible for all catalysts. This particularly refers to the way Pd is introduced, as well as to the solvents and precipitation agents used.

For the co-precipitated Pd/Ga_2O_3 catalyst, 100 mg Pd (Goodfellow Pd foil 99.99%) were dissolved in a mixture of 5 mL HNO_3 (65%) and 1 mL HCl (37%) while gently heating. Subsequently, the volume was increased with distilled H_2O to 50 mL. Separately, 1.5 g Ga (Goodfellow Ga metal 99.9999%) were dissolved in HCl (37%) at 373 K. Both solutions were unified and diluted to 100 mL total volume using distilled H_2O. Afterwards, NaOH (5%) was added dropwise at 353 K until a pH value of 7–8 was reached. The resulting precipitate was allowed to age overnight and subsequently filtrated and dried at 373 K. Remaining Cl was removed by thorough washing. To obtain the pre-catalyst, the powder was calcined in air at 773 K for 4 h (which also removes the remnants of HNO_3 decomposition).

Similarly, the respective co-precipitated Pd/In_2O_3 and Pd–Ga_2O_3–In_2O_3 catalysts were synthesized. For the former, In metal foil (Goodfellow 99.999%) was dissolved in HNO_3 and $In(OH)_3$ precipitated by addition of NaOH (5%). 2.4 g $In(OH)_3$ were then dissolved in 5 mL HCl (37%) and diluted using distilled H_2O up to 20 mL total volume. The Pd-containing solution (preparation exactly as above) was then added and the unified solution treated as the Pd–Ga_2O_3 catalyst above.

The catalyst containing both Ga_2O_3 and In_2O_3 was prepared by unifying the Pd- and Ga_2O_3-containing solutions (preparation as above) with the respective $In(OH)_3$ solution (0.24 g in 5 mL HCl 37%). Further aging, filtration and calcination were performed as above. Impregnated Pd/Ga_2O_3 and Pd/In_2O_3 have been prepared following a classical wet impregnation technique detailed elsewhere [10, 12].

All catalysts were subsequently characterized by X-ray diffraction (XRD) and (high resolution) electron microscopy (HRTEM) prior to and after methanol steam reforming. As the XRD (Figs. 1, 2, detailed discussion in Sect. 3.1.) and subsequent TEM analyses reveal, all three catalysts, after calcination, consist of Ga_2O_3 and In_2O_3 grains decorated with small PdO particles. To ensure similar starting conditions and to induce formation of the intermetallic compound/oxide interface, oxidative treatments (O_2, 1 bar flowing, 673 K) and then activation in hydrogen stream (H_2, 1 bar flowing, Pd–Ga_2O_3: 673 K; Pd–In_2O_3:

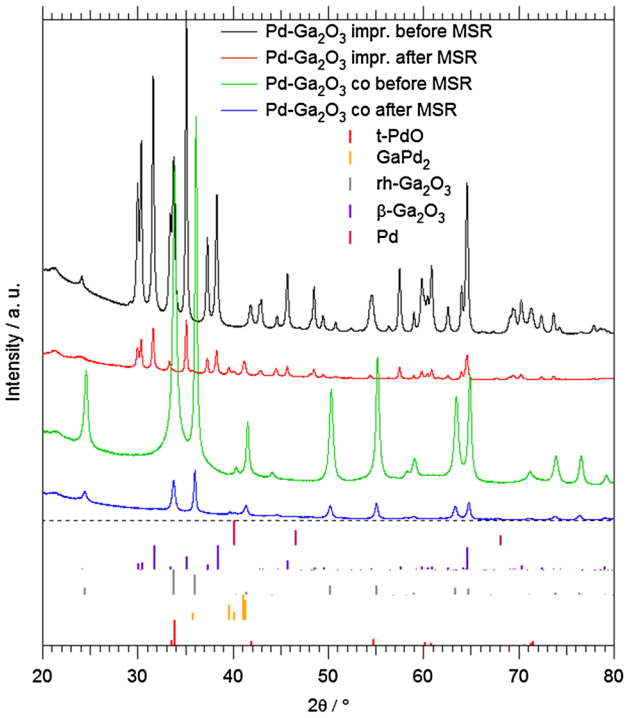

Fig. 1 PXRD data of impregnated and co-precipitated Pd-Ga_2O_3 before oxidation and after the catalytic testing. Reference diffractograms for tetragonal PdO (#43-1024), orthorhombic $GaPd_2$ (#50-1443), rhombohedral Ga_2O_3 (#43-1013), monoclinic Ga_2O_3 (#43-1012) and cubic Pd metal (#46-1043) for phase analysis are shown as vertical bars. Data of the H_2 pre-reduced state (after calcination and before MSR) are almost identical to those after MSR and are therefore not shown

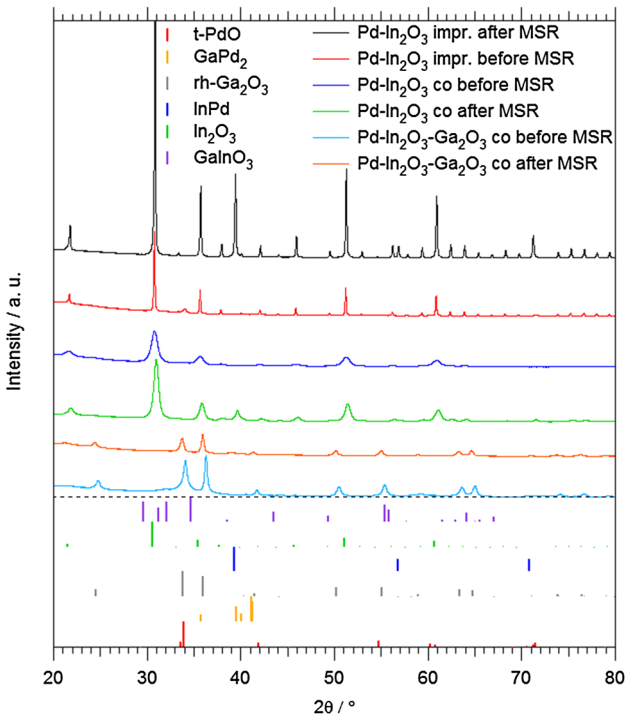

Fig. 2 PXRD data of impregnated and co-precipitated Pd-In_2O_3 and co-precipitated Pd–Ga_2O_3–In_2O_3 before oxidation and after the catalytic MSR run. Reference diffractograms for tetragonal PdO (#43-1024), orthorhombic $GaPd_2$ (#50-1443), rhombohedral Ga_2O_3 (#43-1013), cubic In_2O_3 (#06-0416), hexagonal $GaInO_3$ (#21-0333) and cubic $In_{0.52}Pd_{0.48}$ (#46-1011) for phase analysis are shown as vertical bars. Data of the H_2 pre-reduced state (after calcination and before MSR) are almost identical to those after MSR and are therefore not shown

523 K; Pd–Ga_2O_3–In_2O_3: 473 K) were carried out prior to the actual catalytic measurement. Flow rates between 0.01 and 5.00 mL min^{-1} have been used.

2.2 Catalytic Experiments

For all long-term catalytic measurements, a plug-flow reactor setup (PID Eng&Tech) was used. The flow reactor setup consists of a reactor core, which is represented by a 20 cm long steel cylinder, the inner walls of which are coated by silica to prevent influences by any spurious catalytic activity of steel. The catalyst is positioned within this cylinder using quartz glass wool. The steel tube is further located inside a furnace, allowing temperatures up to 773 K. At the upper gas inlet, a thermocouple is integrated, which extends down into the catalyst bed inside the reactor tube. The reactor itself is connected to the gas supply and discharge ports via Swagelok® quick connectors for easy removal and exchange of catalysts. The gas feed is provided by a constant flow in top-to-bottom direction over the catalyst bed. The gas inlet and outlet are connected to each other by a six-way valve, which serves as a bypass of the reactor section if needed. The various gases are introduced via mass-flow controllers, which makes a wide range of different gas mixtures available. Furthermore, a heated injection valve is located next to the inlet port, which is equipped with a Gilson HPLC pump, enabling liquids to be mixed with the gas stream after vaporization (flow rate 0.01–5.00 mL min^{-1}). Most parts (except for gas analysis and external liquid pump) are placed inside a temperature-controlled area of 393 K to exclude condensation phenomena. For similar reasons, the injector as well as the gas-feed pre-heating unit are kept at elevated temperatures. After passing the reactor section, the gas stream exits the temperature-controlled area and, subsequently, all liquid contents (in this case methanol and water) are removed by a Peltier separating unit in addition to a Nafion© membrane only penetrable for gases. The dry gases are detected by a Varian micro-GC system consisting of three separate chromatography columns for hydrogen, carbon monoxide and carbon dioxide, respectively.

For all experiments, a methanol–water mixture of 1:1 composition was used under flowing conditions. The steam flow was set to 1 mL min^{-1} and mixed with the carrier-gas

stream (8 mL min^{-1} N_2/He mixture, the latter as internal standard) before entering the reactor section. The total pressure in the apparatus is limited to 1 bar. The reactor setup shows no conversion in MSR under the conditions applied.

As for the selectivity, no CH_4 is observed. The CO-selectivity can be obtained by subtracting the selectivity to CO_2 from 100%. Hydrogen selectivity is 100%, since no other hydrogen-containing product is detected.

2.3 Structural Characterization

Powder X-ray diffraction was conducted on a STOE-STADIP-MP powder diffractometer in Bragg–Brentano geometry (Cu $K_{\alpha 1}$-radiation, Ge(111) monochromator) from $2\theta = 5°$ to 100°.

A Philips CM200FEG microscope operated at 200 kV and equipped with a field emission gun, Gatan imaging filter, and an energy-dispersive X-ray (EDX) analyser was used for TEM studies. The coefficient of spherical aberration was Cs = 1.35 mm, and the information limit was better than 0.18 nm. Selected areas were processed to obtain the power spectra (PS, square of the Fourier transform of the image), which were used for measuring interplanar distances (± 0.5%) and angles (± 0.5 deg) for phase identification. Projected areas have been measured and equivalent diameters calculated for a certain number of catalyst particles in each sample; in all cases (except for the impregnated Pd/Ga_2O_3) the values of standard error of the mean diameter were ≤ 0.3 nm. Frequency distributions of particle sizes fitted well to lognormal functions.

3 Results and Discussion

3.1 Structural Characterization

3.1.1 X-ray Diffraction

X-ray diffraction patterns collected for all catalysts before and after the catalytic treatments are highlighted in Figs. 1 and 2. For the impregnated/co-precipitated Pd–Ga_2O_3 catalysts (Fig. 1), similarities but also distinct differences arise. In the state before catalysis (i.e. before hydrogen pre-reduction and after oxidation in air), the impregnated Pd-Ga_2O_3 catalyst is composed of PdO and β-Ga_2O_3, which is expected since impregnation was performed on phase-pure commercial β-Ga_2O_3 powder (black diffractogram in Fig. 1 with majority of reflexes corresponding to lilac bars, PdO best visible at the characteristic split reflex at $2\theta = 34°$). After H_2 pre-reduction and the subsequent long-term presence in the methanol steam reforming mixture, $GaPd_2$ and mainly unaltered β-Ga_2O_3 are detected (red diffractogram). $GaPd_2$ is also found on the co-precipitated catalyst after the pre-reduction/catalytic treatment, but the catalyst support structure before and after catalytic treatment is rhombohedral (α-)Ga_2O_3, which obviously results from the co-precipitation procedure favouring this polymorph. Remarkably, metastable rhombohedral Ga_2O_3 persists during each step of a catalytic cycle, that is, after pre-oxidation, pre-reduction and catalytic treatment (light grey bars/green and blue diffractograms in Fig. 1).

Structurally, the impregnated/co-precipitated Pd–In_2O_3 materials appear less complex (Fig. 2). In both cases, before oxidation, tetragonal PdO/cubic In_2O_3 is present. After the MSR treatment, the structure of the catalysts is characterized as InPd/cubic In_2O_3.

Apparently, the Pd–Ga_2O_3–In_2O_3 catalyst is the crystallographically most complex system (Fig. 2). Before oxidation, weak signals of PdO are present alongside those of cubic In_2O_3 and rhombohedral Ga_2O_3. After catalysis, the latter two are still present, in addition to very weak and broad signals of InPd. $GaPd_2$ is not visible in the XRD patterns, but may partially overlap with the broad InPd reflection at $2\theta = 39°$. It is, however, locally detectable in HRTEM images (*cf.* Fig. 3f). The same is true for the hexagonal ternary oxide $GaInO_3$, detected also by HRTEM, which appears to have formed during the co-precipitation process.

3.1.2 High-Resolution Electron Microscopy

EDX spectra (not shown) taken in 14 different areas reveal the mean ratio of Ga:Pd to be 80:20 ± 4 (std.err.) in the fresh PdO–Ga_2O_3 catalyst after calcination. Analyses of lattice spacings and angles in HRTEM images allow the unambiguous phase identification in most cases (examples are given in Fig. 3g, h, j, k). In general, the structure of the co-precipitated catalyst did not change dramatically during the catalytic reaction, except for the particle size (see Table 1) and their composition. Only some small Pd particles individually supported on rhombohedral gallium oxide (α-Ga_2O_3)—Fig. 3d—or those intermixed with differently sized oxide particles (Fig. 3b) have been observed in the fresh catalyst. Occasionally, amorphous material and gallium oxide particles with the cubic spinel-like structure have been detected. Monoclinic Ga_2O_3 as the thermodynamically most stable Ga_2O_3 polymorph appears to be absent at all stages. During reduction and subsequent reaction, elemental palladium is transformed to $GaPd_2$ with much larger particle size (Fig. 3e, f, h). Frequently, the $GaPd_2$ crystals display {101} and {001} facets (Fig. 3h). The surfaces of the $GaPd_2$ particles are clean and not covered with any overlayers, but in several cases, single crystalline particles displayed inhomogeneous contrast of "core–shell" type (not shown) with darker cores and lighter shells—probably due to depletion of the sub-surface regions with Pd. This is supported by EDX analyses of individual intermetallic particles which show

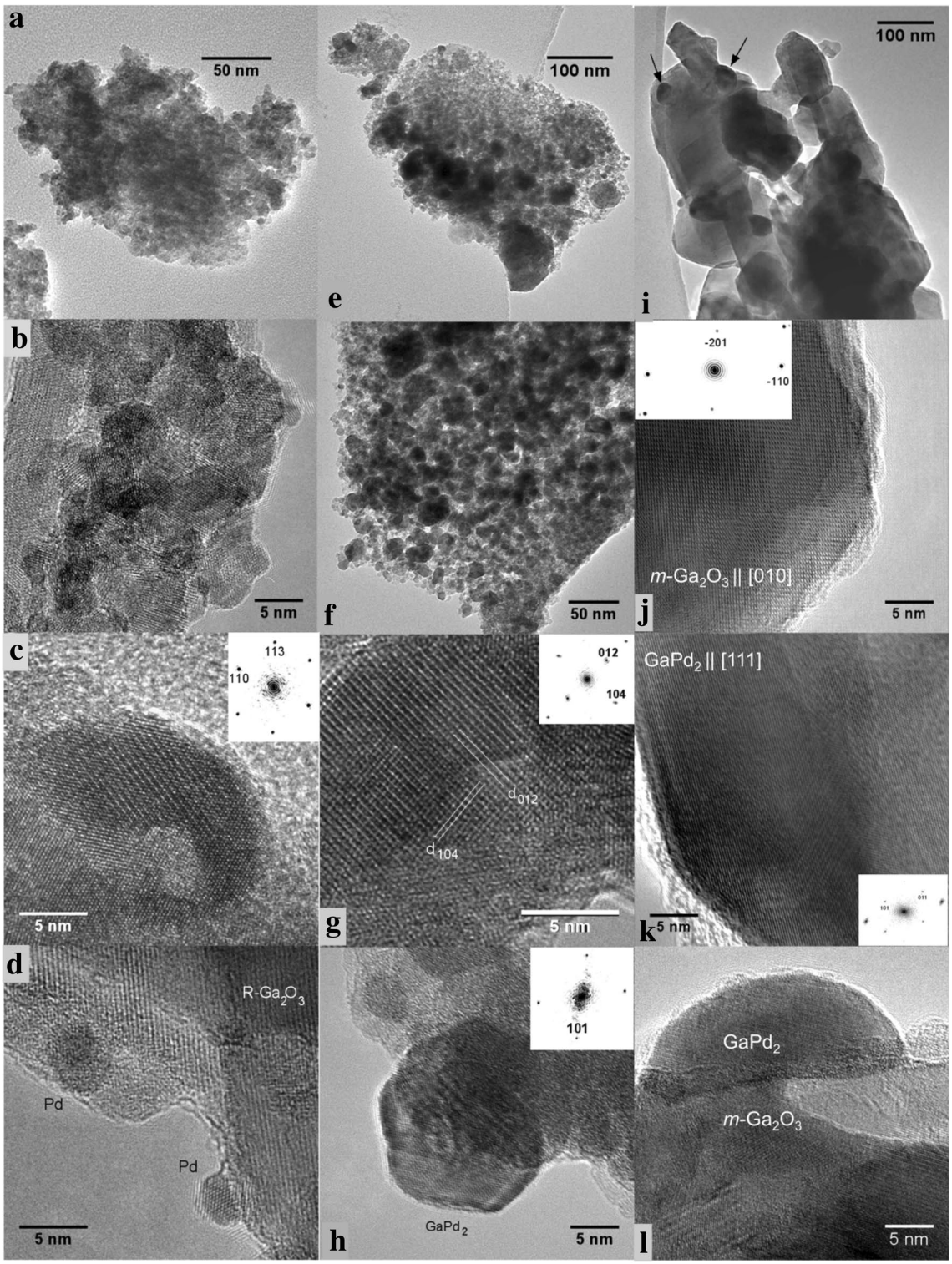

Fig. 3 TEM and HRTEM images of the co-precipitated and impregnated Pd–Ga_2O_3 catalysts: **a**–**d** freshly prepared by co-precipitation and calcination in air at 773 K; **e**–**h** co-precipitated, after the MSR run; **i**–**l** impregnated, after the MSR run. Insets in **c, g, h, j, k** examples of power (FFT) spectra used for phase identification and determination of crystal orientation. Arrows in **i** show some of the $GaPd_2$ particles

Table 1 Overview of the structural and catalytic findings by HRTEM, XRD and methanol steam reforming

Support	Phases (XRD)	Phases (HRTEM)	Ga(In):Pd (EDX)	$D_{vol.wtd}$ (Pd phase), nm (TEM)	Surface area (Pd phase) m^2g^{-1} (TEM)	CO_2 Selectivity (%)	Conversion (%)
Ga_2O_3	**rh-Ga_2O_3/t-PdO**	**rh + c-Ga_2O_3/Pd**		**3.2**	**25.6**		
	rh-Ga_2O_3/$GaPd_2$	rh + c-Ga_2O_3/$GaPd_2$	47:53	18.6	4.4	90	82
	m-Ga_2O_3/$GaPd_2$	*m-Ga_2O_3/$GaPd_2$*	*39:61*	*88.4*	*0.9*	*59*	*58*
In_2O_3	**c-In_2O_3/t-PdO**	**c-In_2O_3/Pd**		**5.6**	**14.7**		
	c-In_2O_3/InPd	c-In_2O_3/InPd	51:49	23.5	3.5	97.5	91
	c-In_2O_3/t-PdO	*c-In_2O_3/InPd, $InPd_2$*	*46:54*	*12.7*	*6.5*	*99*	*50*
Ga_2O_3/In_2O_3	**rh-Ga_2O_3/t-PdO**	**rh-Ga_2O_3/rh-In_2O_3/h-$GaInO_3$/Pd/$GaPd_2$**	n/a	**4.1**	**20.1**		
	rh-Ga_2O_3/t-PdO/InPd	rh-Ga_2O_3/c-In_2O_3/$GaPd_2$/InPd		8.5	9.6	97.5	60

Bold values represents fresh co-precipitated catalyst

Normal values represents co-precipitated catalyst after MSR reaction

Italic values represents impregnated catalyst after MSR reaction

some deficiency of Pd with respect to the stoichiometric ratio Ga:Pd = 1:2 in most cases. Locally, Ga_7Pd_3 is also present as a minority phase in the catalyst after reaction. It is noteworthy that, in contrast to XRD, no Pd oxide was found with HRTEM in neither fresh, nor in the reacted material, probably because of its instability under the electron-beam in high vacuum.

In contrast to the co-precipitated materials, where only rhombohedral Ga_2O_3 was found, in the impregnated catalysts, large single-crystalline particles (sometimes of submicrometer size) of the monoclinic Ga_2O_3 polymorph (with elemental Pd particles decorating them prior to reduction/catalysis) were covered with $GaPd_2$ after reduction/catalysis—Fig. 3i–k. The particles exhibit a tendency to wet the surface of the support, displaying some kind of metal-support interaction—Fig. 3l. On average, the $GaPd_2$ particles are closer to the stoichiometric composition, according to EDX, but nevertheless did not correspond exactly to the nominal formula.

EDX spectra (not shown) taken in eight different areas yield a mean ratio of In:Pd = 83:17 ± 5 (std.err.) in the fresh co-precipitated and calcined Pd-In_2O_3 catalyst. Both phases (elemental Pd and bcc In_2O_3) are well crystallized (Fig. 4a–c); no amorphous material was found. Pd particles are distributed on the In_2O_3 surfaces without clustering. They display clean surfaces, sharp edges and, quite frequently, twin boundaries (Fig. 4b, c)—a feature that is known to increase the activity of Cu in the industrial Cu/ZnO/Al_2O_3 catalyst [25]. In addition to pure Pd, a few particles of $InPd_2$ have been locally detected in the spent impregnated catalyst, highlighting the increased intermixing ability of Pd and In.

In most cases, the identification of Pd-containing phases from HRTEM data is ambiguous for the Pd–In_2O_3 catalyst studied after the MSR run, because of the strongly distorted structure of the particles—especially in the impregnated system—that could probably be caused by non-stoichiometry (variable In/Pd ratio). Nevertheless, the structure of InPd fits the majority of the HRTEM images in the co-precipitated system, and $InPd_2$ for the impregnated catalyst. This is in agreement with XRD (except for $InPd_2$). On average, EDX analyses of individual particles reveal the compositions to be close to the stoichiometric composition of InPd in the co-precipitated catalyst after the reaction, but the In:Pd ratio was shifted towards Pd in the impregnated material. Both types of particles partially exhibit shells of distorted In_2O_3 (Fig. 4e, f, i), which are thicker in the co-precipitated (up to 2 nm), and thinner and less-ordered in the impregnated catalyst.

For the Pd–Ga_2O_3–In_2O_3 system, the composition could be determined by EDX to be Ga:In:Pd = 65:17:18 ± 2 (std. err.) in the fresh Pd–Ga_2O_3–In_2O_3 material. Along with the individual gallium and indium oxides, the hexagonal phase of $GaInO_3$ has been detected with HRTEM in freshly prepared mixed-oxide supported catalyst (Fig. 5a, b). The palladium particles in the fresh catalyst were similar to those in the single-oxide materials: they exhibited a cuboctahedral shape.

After reaction, the majority of Pd-containing particles have been identified as $GaPd_2$ and InPd (or In_xPd_y with probably variable In:Pd ratio)—Fig. 5 b, f–h. The former were typically embedded in an amorphous matrix (similar to Pd in the freshly prepared catalyst)—Fig. 5c, d, g—and displayed shells (also amorphous), but the latter had clean surfaces (Fig. 5h). In the fresh catalyst, several particles of the rhombohedral polymorph of In_2O_3 have been found. Table 1 quickly summarizes the main findings of the XRD

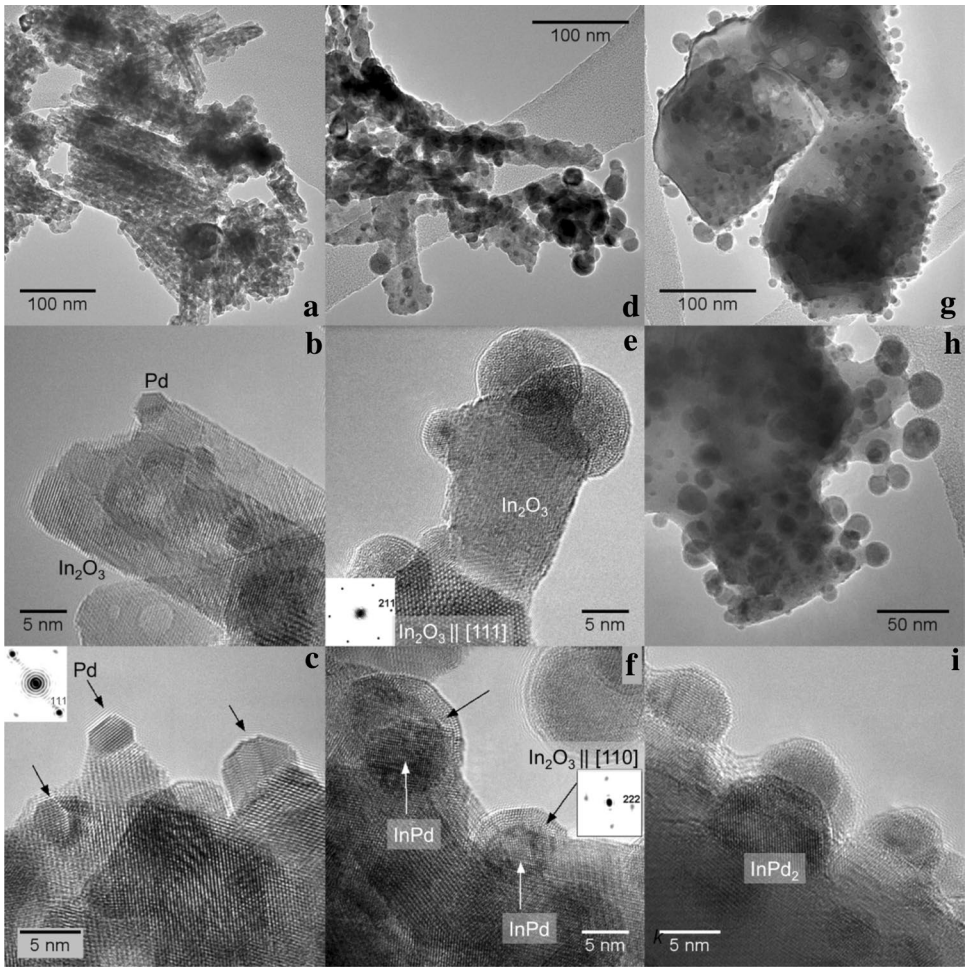

Fig. 4 TEM and HRTEM images of co-precipitated and impregnated Pd–In_2O_3 catalysts: **a**–**c** freshly prepared by co-precipitation and calcination in air at 773 K; **d**–**f** co-precipitated, after the MSR run; **g**–**i** impregnated, after the MSR run. Insets in **c, e, f** examples of power (FFT) spectra used for phase identification and determination of crystal orientation of indicated phases. Black arrows in **c** point to Pd particles, in **f** to In_2O_3 shells on InPd particles. Elemental Pd in the fresh catalyst is due to e-beam reduction of PdO in the electron microscope

and TEM work in direct comparison with the catalytic findings, discussed in Sect. 3.2.

3.2 Catalytic Characterization in Methanol Steam Reforming

The respective catalytic patterns are shown in Fig. 6. For all of the studied catalytic materials, the methanol conversion and CO_2 selectivity are shown as a function of the time-on-stream. To focus on eventual deactivation, long-term experiments up to 12 h time-on-stream have been performed. In order to highlight possible activity and selectivity improvements by the co-precipitation preparation, the catalytic properties are directly compared to those of already well established impregnated materials.

The catalytic data in Fig. 6a for the Pd–Ga_2O_3 materials show that in contrast to the impregnated Pd–Ga_2O_3 catalyst, which exhibits a comparably low activity (58% methanol conversion) and a low CO_2 selectivity (~59%), the co-precipitated Pd-Ga_2O_3 catalyst displays a much higher CO_2 selectivity at around 90% (increasing from 88 to 91% in the course of the reaction), with an at the same time also much improved conversion (82%). Deactivation on the time scale of the experiment is clearly absent for both systems. The observed catalytic patterns are interesting from a structural point of view, since both the HRTEM and the XRD data reveal that in both cases, a $GaPd_2$ phase has formed after reduction/during the catalytic treatment. Slight compositional variations have been monitored, but without structural breakdown of the $GaPd_2$ phases. The results therefore directly prove what has already been derived from corresponding studies on support-free bulk $GaPd_2$ intermetallic compounds:[8] the mere presence of the $GaPd_2$ intermetallic compound is not enough to enable a high CO_2 selectivity in methanol steam reforming. Rather, a synergistic action between intermetallic and oxidic support material must take place to enhance the water splitting capability of the intermetallic-oxide interface. Exactly this beneficial interface seems to be formed by co-precipitation, which then directly gives rise to improved CO_2 selectivity. In the Pd–Ga_2O_3 case, co-precipitation also causes the exclusive formation of a $GaPd_2$-rhombohedral Ga_2O_3 (α-Ga_2O_3) interface, which apparently is also active and selective in methanol steam reforming. The presented catalytic properties of this co-precipitated $GaPd_2$/α-Ga_2O_3 material moreover strongly resemble similar studies of $GaPd_2$/α-Ga_2O_3 catalysts, where

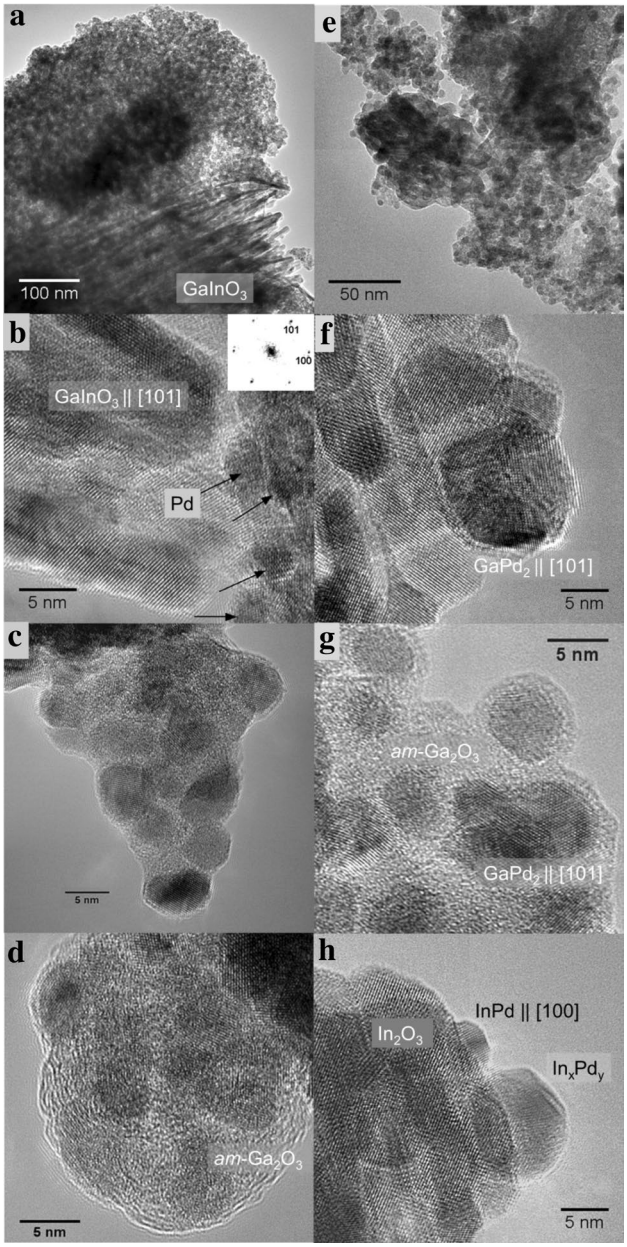

Fig. 5 TEM and HRTEM images of the co-precipitated Pd–Ga_2O_3-In_2O_3 catalyst **a**–**d** freshly prepared by co-precipitation and calcination in air at 773 K; **e**–**h** co-precipitated, after the MSR run. Inset in **b** example of powder spectra used for phase identification and determination of crystal orientation. Black arrows in **b** point to Pd particles. Elemental Pd in the fresh catalyst is due to e-beam reduction of PdO in the electron microscope

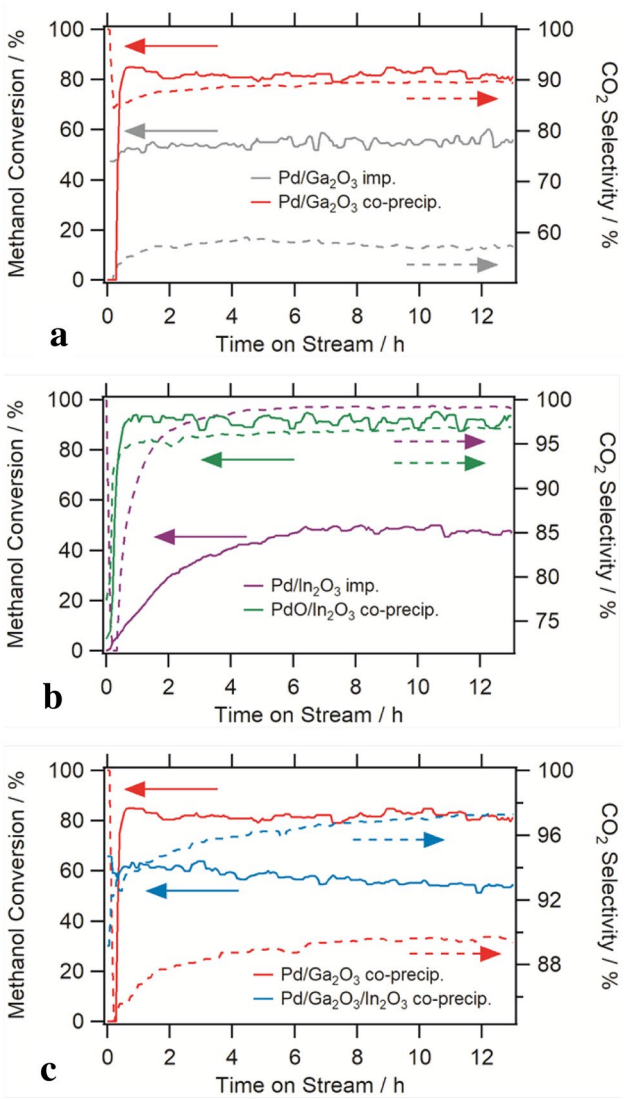

Fig. 6 Comparative methanol steam reforming reaction profiles measured on a set of Pd–Ga_2O_3, Pd–In_2O_3 and Pd–Ga_2O_3–In_2O_3 catalysts. **a** shows the comparison of methanol conversion and CO_2 selectivity vs. time-on-stream between a conventionally impregnated Pd-Ga_2O_3 catalysts and a co-precipitated one. In **b** the same is highlighted for the Pd-In_2O_3 systems. **c** Finally shows the comparison between an In_2O_3-doped Pd–Ga_2O_3 catalyst and an accordingly In_2O_3-free material. Prior to the methanol steam reforming reaction (molar ratio methanol:water = 1:1) at 573 K, pre-oxidation at 673 K in oxygen for 1 h, as well as pre-reduction in hydrogen (1 h) has been performed. Pre-reduction for Pd–In_2O_3 and Pd–Ga_2O_3 523 K, for Pd–Ga_2O_3–In_2O_3 473 K. Solid lines represent conversion, dashed lines refer to CO_2-selectivity

α-Ga_2O_3 was impregnated by small Pd particles and subsequently subjected to hydrogen reduction to induce the formation of $GaPd_2$ intermetallic particles [8]. The increase of activity and selectivity could also be explained by remnants of elemental Pd after pre-reduction, which are successively transformed into $GaPd_2$ during methanol steam reforming (which might be easier if the metal-oxide interface is more extended).

A slightly different pattern is observed for the Pd–In_2O_3 catalysts (Fig. 6b). Here, the structural situation of both co-precipitated and impregnated catalysts is less complex, since, in both cases, after reduction and during catalysis, only cubic In_2O_3 and (compositionally slightly variable) InPd as the main phases are present. This is then directly reflected in the trends of the activity and CO_2 selectivity. In both cases,

CO_2 selectivities of > 95% have been obtained. The methanol conversion of the co-preciptated $InPd/In_2O_3$ catalyst, is however, much higher (90 vs. 40% on the impregnated one).

Finally, Fig. 6c reveals how the CO_2 selectivity of a co-precipitated $GaPd_2/Ga_2O_3$ can be directly improved by promotion with In_2O_3. In comparison to the former, the CO_2 selectivity of the latter can be improved from 90 to almost 98%. The methanol conversion of the In_2O_3-doped material at 60% is somewhat lower than that of the undoped sample (80%) and decreases slightly in the course of the reaction, indicating some deactivation.

4 Conclusions

We have shown how the catalytic properties of already well-established intermetallic methanol steam reforming catalysts on Pd basis, namely $GaPd_2/Ga_2O_3$ and $InPd/In_2O_3$, can be steered and exemplarily improved by a co-precipitation approach to synergistically alter the intermetallic compound-supporting oxide interface. This is especially evident for the $GaPd_2$–Ga_2O_3 catalyst, where the use of co-precipitation gives rise to a selectivity improvement also for the undoped $GaPd_2$ sample, which can be further beneficially influenced by In_2O_3 doping. This improvement can be achieved despite the increased structural complexity and chaotic morphology of the $GaPd_2/InPd/Ga_2O_3/In_2O_3$ material. Apparently, the presence of a variety of distinct support- and intermetallic particle phases is not detrimental to activity/selectivity as long as the appropriate intermetallic phases are present and exhibit optimized intermetallic-support phase boundary dimensions.

Acknowledgements Open access funding provided by Austrian Science Fund (FWF). The work was financially supported by the Austrian Science Fund (FWF) via grants F4503-N16 and it was performed within the research platform “Materials and Nanoscience” at the University of Innsbruck. Assistance from the special PhD program “Reactivity and Catalysis” is also greatly acknowledged.

References

1. Iwasa N, Takezawa N (2003) Top Catal 22:215
2. Palo DR, Dagle RA, Holladay JD (2007) Chem Rev 107:3992
3. Sa S, Silva H, Brandao L, Mousa JM, Mendes B (2010) Appl Catal A 99:43
4. Lorenz H, Rameshan C, Bielz T, Memmel N, Stadlmayr W, Mayr L, Zhao Q, Soisuwan S, Klötzer B, Penner S (2013) ChemCatChem 5:1273
5. Armbrüster M, Behrens M, Föttinger K, Friedrich M, Gaudry E, Matam SK, Sharma HR (2013) Catal Rev 55:289
6. Bayer A, Flechtner K, Denecke R, Steinrück HP, Neyman KH, Rösch N (2006) Surf Sci 600:78
7. Rameshan C et al (2010) Angew Chem Int Ed 49:3224
8. Mayr L et al (2014) J Catal 309:231
9. Friedrich M, Penner S, Heggen M, Armbrüster M (2013) Angew Chem Int Ed 52:4389
10. Lorenz H, Thalinger R, Köck EM, Kogler M, Mayr L, Schmidmair D, Bielz T, Pfaller K, Klötzer B, Penner S (2013) Appl Catal A 453:34
11. Rameshan C et al (2012) J Catal 290:126
12. Penner S, Lorenz H, Jochum W, Stöger-Pollach M, Wang D, Rameshan C, Klötzer B (2009) Appl Catal A 358:193
13. Lorenz H, Penner S, Jochum W, Rameshan C, Klötzer B (2009) Appl Catal A 358:203
14. Stadlmayr W, Huber V, Penner S, Klötzer B, Memmel N (2013) J Phys Chem C 117:19558
15. Haghofer A, Föttinger K, Nachtegaal M, Armbrüster M, Rupprechter G (2012) J Phys Chem C 116:21816
16. Haghofer A, Ferri D, Föttinger K, Rupprechter G (2012) ACS Catal 2:2305
17. Friedrich M, Teschner D, Knop-Gericke A, Armbrüster M (2012) J Catal 285:41
18. Neyman K, Lim KH, Chen ZX, Moskaleva LV, Bayer A, Reindl A, Borgmann D, Denecke R, Steinrück HP, Rösch N (2007) PhysChemChemPhys 9:3470
19. Bera B, Vohs JM (2007) J Phys Chem C 111:7049
20. Penner S, Jenewein B, Gabasch H, Klötzer B, Wang D, Knop-Gericke A, Schlögl R, Hayek K (2006) J Catal 241:14
21. Rameshan C et al (2010) J Catal 276:101
22. Rameshan C, Lorenz H, Zemlyanov D, Arrigo R, Hävecker M, Blume R, Knop-Gericke A, Schlögl R, Klötzer B, Penner S (2012) J Catal 295:186
23. Lorenz H, Lebedev O, Turner S, Klötzer B, Penner S (2010) Appl Catal A 374:180
24. Neumann M, Teschner D, Knop-Gericke A, Reschetilowski W, Armbrüster M (2016) Chin J Catal 340:49
25. Behrens M, Studt F, Kasatkin I, Kühl S, Hävecker M, Abild-Pedersen F, Zander S, Girgsdies F, Kurr P, Kniep B, Tovar M, Fischer RW, Norskov JK, Schlögl R (2012) Science 336:893

Affiliations

Christoph Rameshan[1,3,5] · Harald Lorenz[1] · Marc Armbrüster[2] · Igor Kasatkin[3,4] · Bernhard Klötzer[1] · Thomas Götsch[1] · Kevin Ploner[1] · Simon Penner[1]

[1] Institute of Physical Chemistry, University of Innsbruck, Innrain 52c, 6020 Innsbruck, Austria

[2] Institute of Chemistry, Technical University Chemnitz, Straße der Nationen 62, 09111 Chemnitz, Germany

[3] Department of Inorganic Chemistry, Fritz-Haber Institute of the Max-Planck-Society, Faradayweg 4-6, 14195 Berlin, Germany

[4] Present Address: Saint Petersburg State University, Universitetskaya nab. 7-9, St. Petersburg, Russia 199034

[5] Present Address: Institut für Materialchemie, Technische Universität Wien, Getreidemarkt 9/BC/01, 1060 Vienna, Austria